coatings

MDPI

Article

Effects of Substrates on Thin-Film Growth of Nickel Zinc Ferrite by Spin-Spray Deposition

Hai Liu [1,2,*], Zhong Yu [2], Xinglian Song [3], Maojun Ran [2], Xiaona Jiang [2], Zhongwen Lan [2] and Ke Sun [2]

[1] Hubei Key Laboratory of Low Dimensional Optoelectronic Materials and Devices, School of Physics Electronic Engineering, Hubei University of Arts and Science, Xiangyang 441053, China
[2] School of Materials and Energy, University of Electronic Science and Technology of China, Chengdu 610054, China
[3] Shandong Chunguang Magnetoelectric Technology Co., Ltd., Linyi 276017, China
* Correspondence: xiaomingever@gmail.com

Abstract: In certain applications, such as on-chip integrated inductors, ferrite materials are highly desirable owing to their superior magnetic and insulation properties. Spin-spray deposition is a promising method for producing high-quality thin films of ferrite, as it does not require a vacuum and can operate at low temperatures. A comprehensive analysis was conducted to investigate the influence of the substrate on the microstructure and magnetic properties of the thin films, and the growth mechanism of this phenomenon was discussed. In addition, first-order reversal curve measurements were used to study the coercivity and grain size distribution. The results indicate that thermal conductivity played a significant role in determining the thin-film growth during spin spray deposition. Polyimide is considered a more suitable substrate under this process due to its appropriate thermal conductivity, which results in more uniform grain distribution and improved magnetic properties, with maximum permeability and a cutoff frequency reaching 55 and 485 MHz, respectively. Our results provide valuable insights into the mechanism of spin-spray deposition and offer an effective way to tune the performance of ferrite thin-film materials.

Keywords: magnetic thin film; anisotropy; spin spray deposition; substrate; ferrite

Citation: Liu, H.; Yu, Z.; Song, X.; Ran, M.; Jiang, X.; Lan, Z.; Sun, K. Effects of Substrates on Thin-Film Growth of Nickel Zinc Ferrite by Spin-Spray Deposition. *Coatings* **2023**, *13*, 690. https://doi.org/10.3390/coatings13040690

Academic Editor: Alina Pruna

Received: 3 March 2023
Revised: 19 March 2023
Accepted: 23 March 2023
Published: 28 March 2023

1. Introduction

In recent years, soft ferrimagnetic materials have garnered significant attention for their exceptional performance in high-frequency applications, particularly in telecommunications. Ferrite materials, particularly in thin-film form, are predominantly utilized due to their exceptional magnetic permeability and elevated resistivity [1–7]. Their strong insulating properties effectively reduce eddy current losses due to skin effects in GHz frequency applications. Integration with ferrite materials also leads to on-chip inductors with higher quality factors than metallic magnetic films. Therefore, ferrite materials are an attractive option for telecommunications applications that require high-performance and low-loss components.

While conventional technologies such as pulsed laser deposition and sputtering have been used in thin-film manufacturing, they have several drawbacks, including the need for high annealing temperatures to achieve crystallization [8–11], limited deposition areas, and low deposition rates of approximately 10 nm/min. As a result, the spin-spray deposition technique proposed by M. Abe has garnered widespread research interest as a novel deposition process for ferrite thin films [12,13]. This technique can be operated at a low temperature of approximately 100 °C in the absence of a vacuum and offers high deposition rates of up to 100 nm/min [14,15]. It is also compatible with various substrates such as glass, silicon, and plastic [16,17]. Thus, the spin spray deposition technique is an attractive option for ferrite thin-film manufacturing due to its efficiency, versatility, and ease of use.

O. Obi deposited spin-sprayed $Ni_{0.27}Zn_xFe_{2.73-x}O_4$ (where x = 0.03~0.1) thin films onto glass substrates under a 360 Oe external magnetic field, and the films exhibited a

permeability of 50 at 1 GHz [18]. By changing the pH value of the metallate and oxidant, the effect of the process parameters of the spin spray deposition on the microstructure and magnetic properties of the nickel zinc ferrite thin film was studied. High permeability ($\mu_r' > 200$ @ 0.5 GHz) with low loss ($\tan\delta_m$ ~0.027) in the range of 3 to 5 GHz was fulfilled when the pH value of metallate was 4.6 and the pH value of oxidant was 9.6 [19]. Afterward, the inductance and quality factor of the inductor integrated with the film at the GHz frequency are significantly improved compared with the air-core one. In addition, the maximum quality factor of the solenoid inductor reached 23, which was a relatively high reported performance [20].

Ray et al. conducted comprehensive research aimed at optimizing the deposition process of ferrite thin films by examining various pertinent parameters. They demonstrated that the proposed μ-droplet deposition regime resulted in an increased Snoek's product in comparison to the continuous liquid layer regime. The optimal Snoek's product was obtained when the oxidant had a pH of 8.28. Furthermore, by employing Lorentz TEM, the magnetic domains of NiZnCo ferrite were visualized, and the presence of multi-grain domains in spin-sprayed thin films was experimentally observed for the first time. [21].

While there have been significant recent research efforts on the study of spin-spray deposition for ferrite thin-film manufacturing, there are still several unresolved issues. The hypothesis about the film-growth mechanism in spin-spray deposition has not been directly verified by experimental results. Furthermore, prior studies employed various substrates without extensively examining their influence on the magnetic properties of thin films. In fact, the effect of the substrate plays an important part in tuning the structural and magnetic characteristics of ferrite thin films [22–24].

As a critical component of integrated passive devices such as on-chip inductors, magnetic thin films face diverse substrate requirements. Common substrates in semiconductor processes, such as silicon compounds and glass, are often used for integrated circuit substrates. However, for spin-spray deposition, the adhesion and thermal conductivity of the substrate can significantly affect the performance of the thin film. This study investigates the impact of substrates on high-performance ferrite thin films using a self-developed ultrasonic spray system and explains the film formation mechanism in-depth, providing valuable references for new generations of integrated passive devices.

2. Materials and Methods

NiZnCu ferrite thin films were fabricated using a self-designed spin-spray deposition system based on Sono-Tek ultrasonic atomizing solution. The oxidation solution, containing 5 mM/L $NaNO_2$ and 20 mM/L CH_3COONa, and the precursor solution, consisting of $NiCl_2$, $ZnCl_2$, and $FeCl_2$ dissolved separately in deionized water, were sprayed through ultrasonic atomizing nozzles onto 0.2 mm thick substrates, including glass, polyimide, SiN, and SiO_2. The substrates were fixed onto a spinning heating plate using a vacuum pneumatic sucker and heated to 95 °C to produce thin films with a composition of $Ni_{0.2}Zn_{0.1}Fe_{2.70}O_4$ at a growth rate of 30~100 nm/min.

The ferrite thin films were characterized using various techniques, including X-ray diffraction (XRD) measurements using a Maxima-X XRD-7000 (Shimadzu, Kyoto, Japan) with Cu-Kα radiation, microstructural imaging using scanning electron microscopy (FE-SEM, JEOL JSM-7800F, JEOL, Tokyo, Japan), contact angle measurements using Biolin Theta Flex (Biolin Scientific, San Diego, CA, USA), room temperature magnetization measurements using a vibrating sample magnetometer (Lake Shore 8604, Lake Shore Cryotronics, Westmont, IL, USA) including FORCs and hysteresis loops, infrared thermal imaging using a Fotric 220 series thermal camera, and permeability spectrum testing using an Agilent N5227A PNA network analyzer (Agilent Technologies, Santa Clara, CA, USA) with a fixture based on the principle of the shorted microstrip method. These characterization techniques provide insights into the structural, magnetic, and physical properties of the ferrite thin films and can help guide future optimization efforts [25,26].

3. Results

Figure 1 depicts the XRD results of the nickel zinc thin films on different substrates. The fine crystallization of the ferrite thin films was indicated by the characteristic peaks of typical spinel structures. The Scherrer formula was used to calculate the average crystallite diameters (d) of four specimens [27]:

$$L = \frac{0.9\lambda}{\beta \cos\theta}, \tag{1}$$

where λ is 0.15408 nm for the wavelength of CuKa radiation, θ is the Bragg angle, and β equals $B - b$. B represents full-width at half maximum while b is the line broadening originated from the instrument. Since the formula only applies to grains smaller than 200 nm, the latter two samples cannot be accurately estimated.

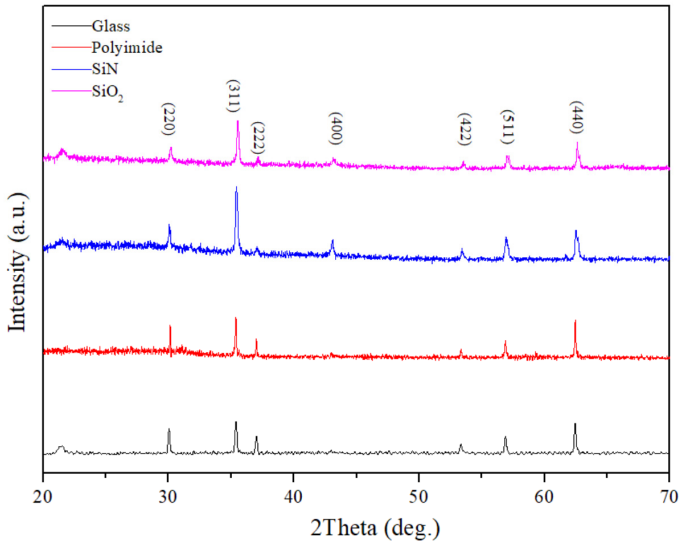

Figure 1. X-ray diffraction results of spin-sprayed films on different substrates.

The presence of a preferred (222) characteristic peak in ferrite thin-film samples deposited on glass and polyimide substrates indicates a specific crystallographic alignment. To better understand this abnormal orientation, Figure 2 illustrates the crystalline structure of the spinel unit cell, featuring a face-centered configuration of A sites for metallic cations, represented by silver spheres. The unit cell contains eight A sites with metallic cations coordinated by four oxygen atoms, and sixteen B sites with metallic cations surrounded by six oxygen atoms, portrayed as golden spheres in the figure [28].

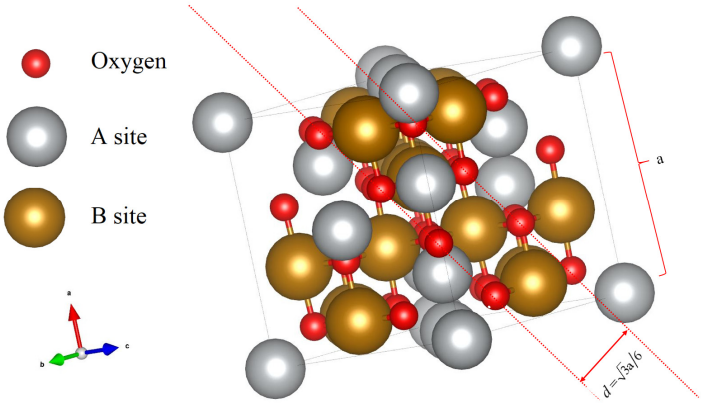

Figure 2. Schematic representation of the spinel ferrite crystal structure.

Figure 2 highlights the close-packing facet (*hhh*) of O^{2-} with a dashed line and shows the interplanar distance d (= $\sqrt{3}a/6$, the same for B sites) that is readily determined through geometric calculations. Utilizing the equation for lattice spacing in cubic structures, the lattice parameter can be subsequently calculated:

$$d = \frac{a}{\sqrt{h^2 + k^2 + l^2}}, \tag{2}$$

X-ray diffraction reveals that h equals 2. This indicates that grains featuring the (222) lattice face aligned parallel to the substrate made the dominant contribution to the growth of the ferrite thin film. To provide further insight, FESEM was employed to investigate the microstructure of all samples, as illustrated in Figure 3.

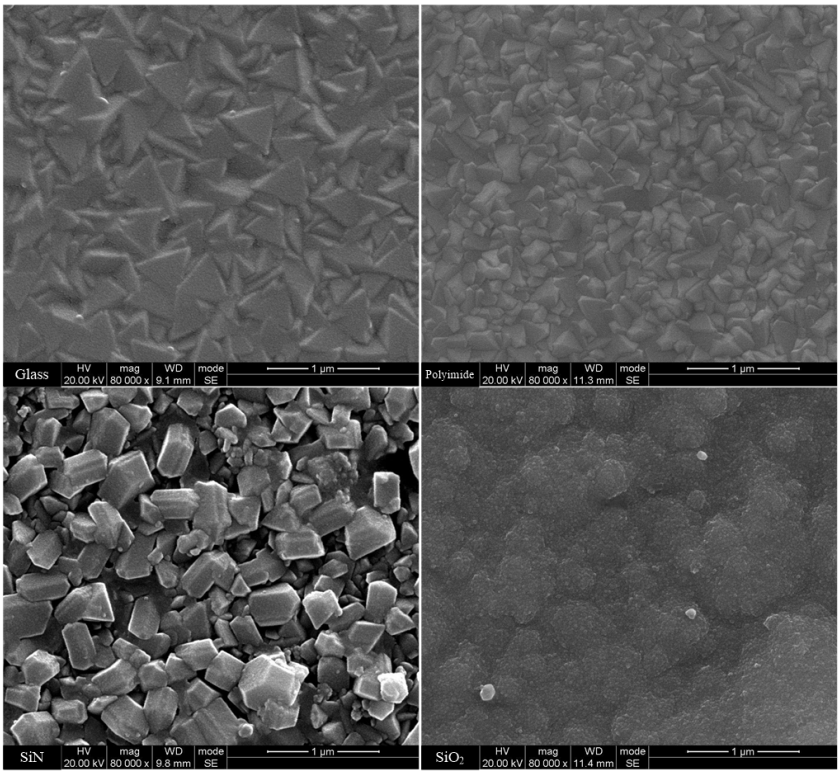

Figure 3. FESEM micrographs of spin-sprayed ferrite thin films on various substrates.

The X-ray diffraction analysis revealed that grains with a lattice face (222) grown parallel to the substrate were predominant in the ferrite thin films, with *h* equaling 2, due to the triangular cross-section of the {*hhh*} crystal plane in the cubic crystal. Figure 3 illustrates the microstructure of all samples, as examined using FESEM.

Although all samples were prepared with the same composition and deposition process, the microscopic photos revealed distinct morphology. The thin film on glass substrate presented triangular grains. As stated in the determined (222) preferred orientation, and the cross-section along the {*hhh*} crystal plane in the cubic crystal will be a triangular shape; thus, these triangular grains can be easily understood.

The (222) facet orientation preference and triangular grain microstructure provide direct evidence for understanding the atomic-level growth kinetics of thin films during spin-spray deposition. This information helps resolve long-standing questions about the deposition mechanism of spin-sprayed films and supports earlier hypotheses on ferrite thin-film growth [29]. The initial layer forms as the substrate absorbs ferrous ions from the sprayed droplets and these cations associate with OH^-. Upon heating and oxidation by NO^{2-}, the absorbed ions convert to trivalent iron ions (B sites), while the adjacent OH^- dehydrates, forming the second layer of the thin film. This process leaves uncoordinated

oxygen bonds to capture new cations, creating a new initial layer, and the cycle continues. Other cations (A sites) contribute to the close-packed formation of spinel ferrite, following the principle of minimum energy.

To assess the strength of orientation, the percentage of the (222) facet was determined employing the Lotgering factor [30–32]:

$$f_L = \frac{P - P_0}{1 - P_0} \quad (3)$$

where $P = \frac{\sum I_{(222)}}{\sum I_{(hkl)}}$ for (222) preferred oriented sample and $P_0 = \frac{\sum I_{0(222)}}{\sum I_{0(hkl)}}$ for the randomly oriented sample. Then, XRD peaks in the 2theta range of 20°–70° were utilized for calculation. The calculated proportions of the (222)-facet of glass and polyimide substrate are 0.26 and 0.22, respectively. It is worth noting that the samples without preferred orientation had a higher deposition rate.

To explore the potential causes of substrates affecting film growth, the wettability (contact angles) and thermal conductivities of different substrates were compared and analyzed. Figure 4 shows the contact angles of the reaction solution used to spin-spray ferrite thin films onto different substrates. As the parameters listed in Table 1 showed [33], no direct relationship between microstructure and conduct angle was observed, which is inconsistent with some conclusions obtained in previous studies. In contrast, the thermal conductivity had a decisive impact on the growth of the film. To visualize the effect of thermal conductivity on the reaction conditions, the real-time temperature of the substrate surface during the reaction was measured and is presented in Table 1 and Figure 5. The average grain size and deposition rate have a linear dependence on the thermal conductivity: as thermal conductivity increases, they increase monotonously. Unfortunately, the deposition rate was increased at the expense of bad adhesion compared with the (222)-oriented thin film. A reasonable interpretation is that the excessively high thermal conductivity causes the reaction to diffuse from the substrate surface into the infiltrating droplets, causing ferrite to crystallize in the droplets, resulting in a high deposition rate and poor adhesion of the thin film.

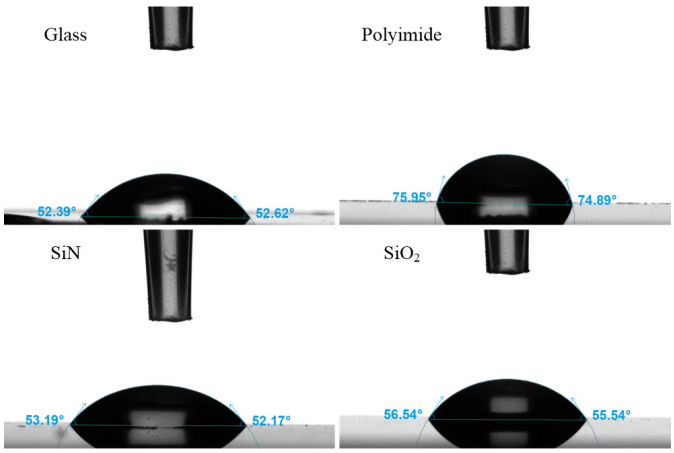

Figure 4. Contact angles of spin-sprayed ferrite thin films on various substrates.

Table 1. Crystalline structural parameters of the spin-sprayed ferrite thin films with different substrates.

Substrate Type	a (Å)	Grain Diameter (nm)	Growth Rate (nm/min)	Contact Angle (°)	Thermal Conductivity ($W \cdot m^{-1} \cdot K^{-1}$)	Temperature (°C)
Glass	8.4100	148.3 ± 22.3	52	52.51	0.8	92.3
Polyimide	8.4089	64.1 ± 7	42	75.42	0.2	91.5
SiN	8.4103	>200	93	52.68	124.6	95.0
SiO_2	8.4104	>200	72	56.04	1.2	94.3

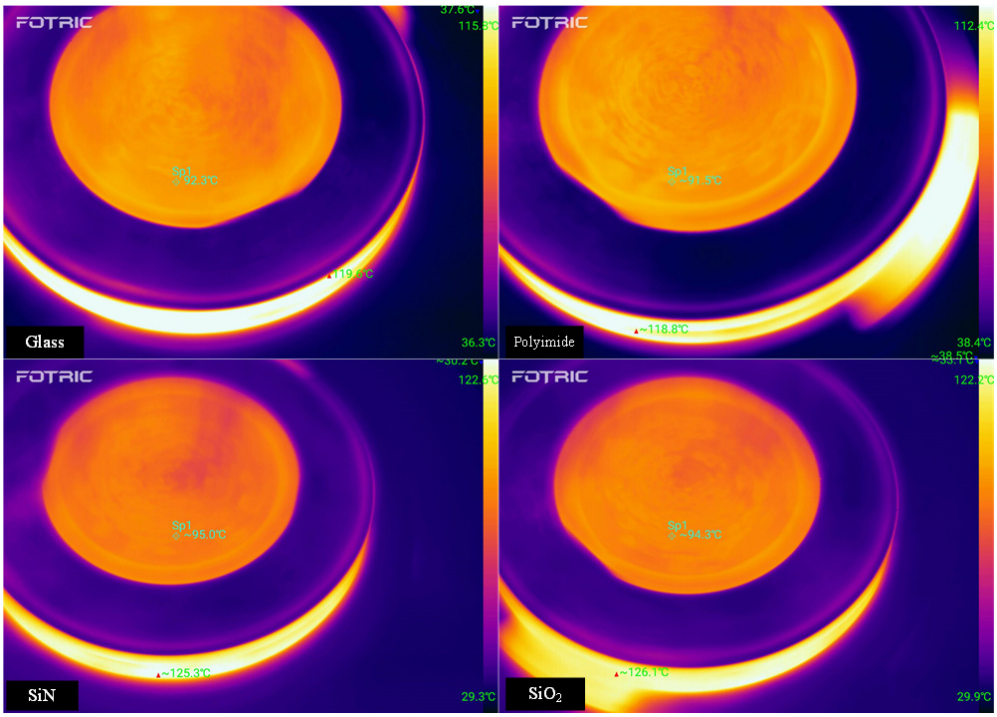

Figure 5. The surface temperature of the spin-sprayed ferrite thin films on various substrates.

Table 2 presents the saturation magnetization (M_s) values for the different substrates, highlighting that the types of substrates considerably impact the values of saturation magnetization. Hysteresis loops for the spin-sprayed ferrite thin films on various substrates are presented in Figure 6. For identical chemical composition, the experimental saturated magnetization is a result of the simultaneous impacts of several factors such as densification and cation distribution. The pronounced variations in M_s may be attributed to the redistribution of cations in the spinel sub-lattice. As is well known, the intensity of XRD is mainly determined by the cation distribution despite the preferred orientation. Based on the XRD results in Figure 1, an obvious redistribution of cations could be predicted.

Table 2. Magnetic properties of the spin-sprayed ferrite thin-film samples.

Substrate Type	M_s (KA/m)	H_c (Oe)	f_r (MHz)	μ'_{max}
Glass	441	23	465	44
Polyimide	445	46	485	55
SiN	402	40	853	38
SiO_2	315	31	1215	22

The coercivity, as an extrinsic attribute, exhibited a considerably intricate change pattern. Among the substrates, except for glass, H_c presented a declining trend that is closely relevant to microstructure in accordance with the random anisotropy model [34,35]. As theoretically described, the coercive force of the ferrite thin film can be determined according to the relationship between the exchange length L_{ex} and the grain size d:

$$\text{(i) Small grain size } (D < L_{ex}): \; H_c = \frac{K_1^4 d^6}{\mu_0 M_s A^3}; \tag{4}$$

$$\text{(ii) Large grain size} (D > L_{ex}): \; H_c = \frac{(AK_1)^{1/2}}{\mu_0 M_s d}. \tag{5}$$

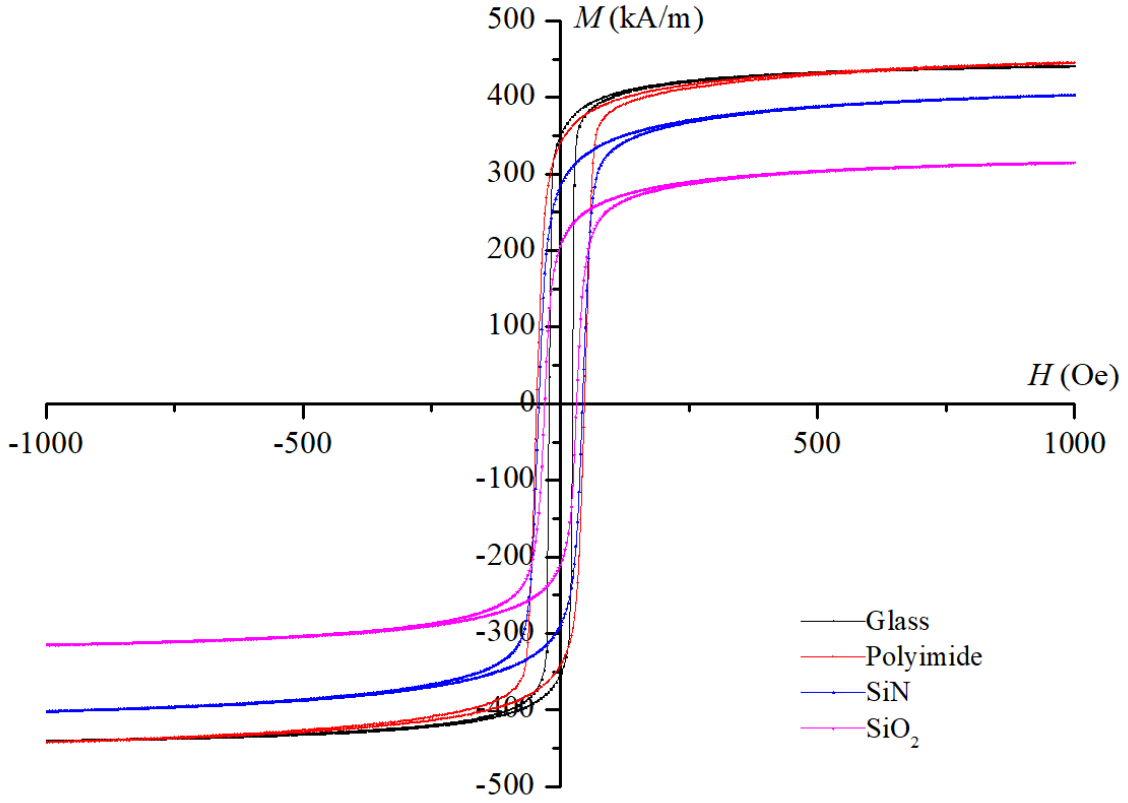

Figure 6. Hysteresis loops for the spin-sprayed ferrite thin films on various substrates.

The exchange length, defined as $L_{ex} = (A/K_1)^{1/2}$, is determined by the stiffness of exchange (A) and the anisotropic constant (K_1). The decreasing trend in H_c with increasing grain size indicates that all samples belong to the $D > L_{ex}$ case. It should be noted that the random anisotropy model does not consider factors such as inner stress and grain shape, which results in abnormal changes for thin films deposited on glass. In fact, samples with a more uniform microstructure exhibit smaller H_c. To accurately assess the influence of inner stress and grain shape, first-order reversal curves (FORC) measurement was performed to quantify the grain size distribution of all samples.

To complete the FORC test, one needs to measure the first-order reversal curve, and then convert it into a FORC diagram that can display the coercive force distribution [36,37].

At the starting point of FORC measurement, the sample was saturated by a large magnetic field set at 500 Oe in this work. The magnetic field is decreased to the specific reverse magnetic field (H_b) and then increases from H_b back to the original saturation. This process generated a curve describing the hysteresis effect at the reversal point H_b. The magnetization point at the external magnetic field $H_a > H_b$ on the curve is denoted as the magnetization point $M(H_a, H_b)$, which is located inside the main hysteresis loop. For any H_a in the hysteresis region, there is an entire internal point group such as $M(H_a, H_b)$, which is categorized by their corresponding FORC reverse magnetic field H_b.

Subsequently, the FORC curve was transformed by calculating the second derivative of the function $M(H_a, H_b)$ related to the external fields H_a and H_b:

$$\rho_{ab}(H_a, H_b) = -\frac{1}{2}\frac{1}{M_s}\frac{\partial^2 M(H_a, H_b)}{\partial H_a \partial H_b} \quad (6)$$

The distribution ρ_{ab} in the formula is defined as the derivative of $M(H_a, H_b)$. When (H_a, H_b) is drawn as a contour, the coordinates were altered from (H_a, H_b) to $H_c = (H_b - H_a)/2$ and $H_u = (H_b + H_a)/2$, which will cause the FORC distribution to behave as follows:

The distribution ρ_{ab} in the formula is the derivative of $M(H_a, H_b)$. To create a contour plot, the coordinates were transformed from (H_a, H_b) to $H_c = (H_b - H_a)/2$ and

$H_u = (H_b + H_a)/2$. This transformation results in the FORC distribution behaving in the following way.

$$\rho_{ab}(H_a, H_b) = \rho_{ab}(H_a(H_c, H_u), H_b(H_c, H_u)) \equiv \rho(H_c, H_u) \quad (7)$$

Data processing was performed using a custom Matlab script, and the resulting FORC diagrams are presented in Figure 7. The relationship between the distribution of coercivity and grain size was identified through the utilization of the random anisotropy model. The presented diagram reveals a unique coercive force distribution for samples with an oriented structure deposited on a glass substrate. This result supports previous findings that a uniform microstructure results in a narrower grain size distribution and lower coercivity.

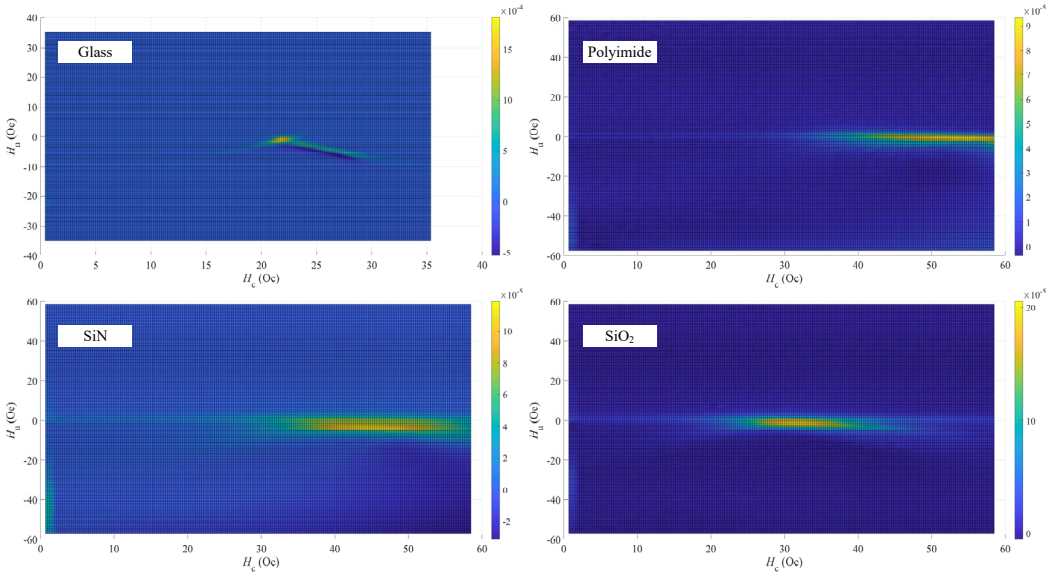

Figure 7. FORC diagrams of the spin-sprayed ferrite thin films with different substrates.

It is important to note that micromorphology can have a substantial impact on the permeability of the material, which can ultimately affect the cut-off frequency. Figure 8 displays the permeability spectra of the four specimens, with the real and imaginary parts presented separately.

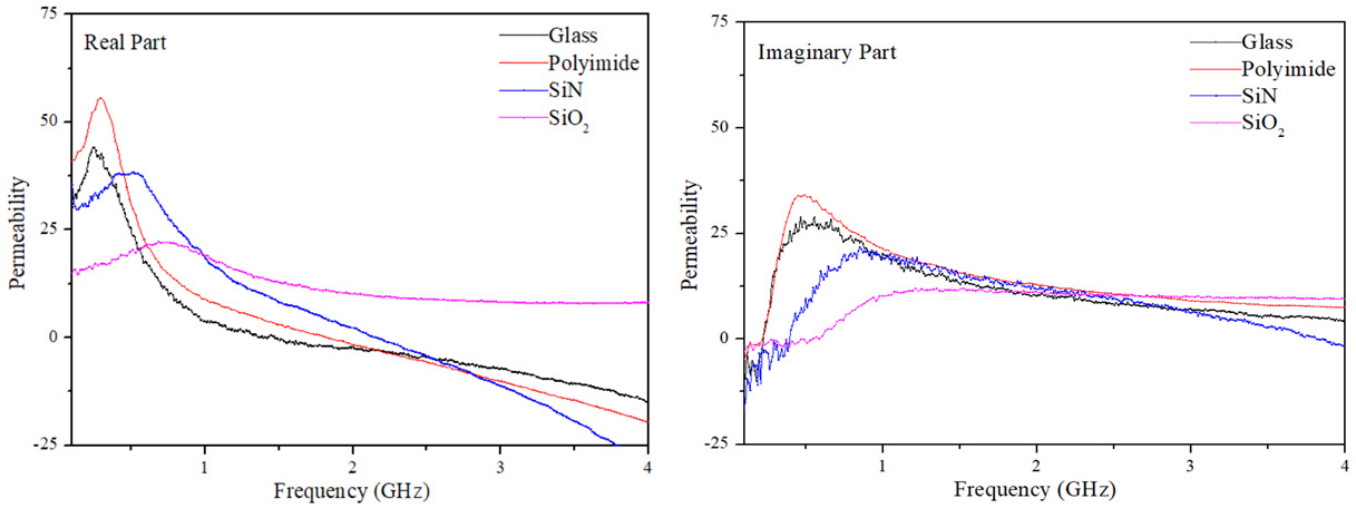

Figure 8. Permeability spectra of the ferrite thin films spin-sprayed on different substrates.

The Archer equation states that the maximum real part of permeability is inversely proportional to the cutoff frequency [38]. Two magnetization mechanisms, domain rotation,

and domain wall motion, exhibit different rules of change concerning grain size: (i) domain rotation $\mu_i \approx \frac{\mu_0 M_s^2}{3\langle K \rangle} = \frac{\mu_0 M_s^2 A^3}{3K_1^4 D^6}$, and (ii) domain wall motion $\mu_i \approx \frac{\mu_0 M_s^2 A^3}{K_1^4 D^6}$ [39]. In both cases, permeability is inversely related to grain size. The results confirm that the thin film deposited on the SiO_2 substrate has a larger grain size than that on the SiN substrate, consistent with the results of the coercivity. Furthermore, as the formulas above demonstrate, the domain wall motion mechanism renders a permeability three times the value of domain rotation under the same condition. A change in grain size can cause the microstructure of a material to transition from a single magnetic domain state to a multi-domain structure, resulting in a corresponding shift in the contribution of the magnetization mechanism. This explains why the magnetic permeability of the sample on the SiN substrate exhibits a small decrease for much larger grains compared to that on the glass substrate.

4. Conclusions

Based on the analysis of microstructure and magnetic properties, it can be inferred that thermal conductivity is a critical factor in determining the spin spray deposition process. The microstructure and magnetic properties of nickel zinc ferrite are affected by the thermal conductivity of the substrate. Excessive heat conduction causes the crystallization of ferrite to shift from the surface, and the chemical reaction occurs in droplets above the expected temperature, resulting in a higher deposition rate and larger grain size, but deteriorated magnetic properties. First-order reversal curve measurements revealed a narrower grain size distribution for uniform samples with preferred orientation. The study revealed that, among the listed Si compounds in the paper, polyimide is considered a more suitable substrate under this process due to its appropriate thermal conductivity, resulting in more uniform grain distribution and improved magnetic properties, with maximum permeability and cutoff frequency reaching 55 and 485 MHz, respectively.

Author Contributions: Conceptualization, H.L.; Data curation, H.L.; Investigation, X.J.; Methodology, X.S. and M.R.; Project administration, Z.Y.; Supervision, K.S.; Writing—Original draft, H.L.; Writing—Review and editing, Z.Y. and Z.L. All authors have read and agreed to the published version of the manuscript.

Funding: This research received no external funding.

Institutional Review Board Statement: Not applicable.

Informed Consent Statement: Not applicable.

Data Availability Statement: Not applicable.

Conflicts of Interest: The authors declare no conflict of interest.

References

1. Hao, A.; Ismail, M.; He, S.; Qin, N.; Huang, W.; Wu, J.; Bao, D. Improved Unipolar Resistive Switching Characteristics of Au-Doped Nickel Ferrite Magnetic Thin Films for Nonvolatile Memory Applications. *J. Alloy Compd.* **2018**, *732*, 573–584. [CrossRef]
2. Abdellatif, M.H.; Azab, A.A.; Moustafa, A.M. Dielectric Spectroscopy of Localized Electrical Charges in Ferrite Thin Film. *J. Electron. Mater.* **2018**, *47*, 378–384. [CrossRef]
3. Harris, V.G. Modern Microwave Ferrites. *IEEE Trans. Magn.* **2012**, *48*, 1075–1104. [CrossRef]
4. Sahu, B.N.; Venkataramani, N.; Prasad, S.; Krishnan, R. Effect of Thickness on Magnetic and Microwave Properties of RF-Sputtered Zn-Ferrite Thin Films. *AIP Adv.* **2017**, *7*, 056102. [CrossRef]
5. Chen, Z.; Harris, V.G. Ferrite Film Growth on Semiconductor Substrates towards Microwave and Millimeter Wave Integrated Circuits. *J. Appl. Phys.* **2012**, *112*, 081101. [CrossRef]
6. Sai, R.; Vinoy, K.J.; Bhat, N.; Shivashankar, S.A. CMOS-Compatible and Scalable Deposition of Nanocrystalline Zinc Ferrite Thin Film to Improve Inductance Density of Integrated RF Inductor. *IEEE Trans. Magn.* **2013**, *49*, 4323–4326. [CrossRef]
7. Wang, G.; Liu, H.; Wu, H.; Li, X.; Qiu, H.; Yang, Y.; Qu, B.; Ren, T.-L.; Han, X.; Zhang, R.; et al. Epitaxial Yttrium Iron Garnet Film for Fabrication of High Frequency On-Chip Inductors. *Appl. Phys. Lett.* **2016**, *109*, 162405. [CrossRef]
8. Nur-E-Alam, M.; Vasiliev, M.; Belotelov, V.; Alameh, K. Properties of Ferrite Garnet (Bi, Lu, Y)3(Fe, Ga)5O12 Thin Film Materials Prepared by RF Magnetron Sputtering. *Nanomaterials* **2018**, *8*, 355. [CrossRef]
9. Zhong, X.; Phuoc, N.N.; Soh, W.T.; Ong, C.K.; Li, L. Dynamic Magnetization of NiZn Ferrite Doped FeSiAl Thin Films Fabricated by Oblique Sputtering. *J. Magn. Magn. Mater.* **2017**, *432*, 373–381. [CrossRef]

10. Emori, S.; Gray, B.A.; Jeon, H.-M.; Peoples, J.; Schmitt, M.; Mahalingam, K.; Hill, M.; McConney, M.E.; Gray, M.T.; Alaan, U.S.; et al. Coexistence of Low Damping and Strong Magnetoelastic Coupling in Epitaxial Spinel Ferrite Thin Films. *Adv. Mater.* **2017**, *29*, 1701130. [CrossRef]
11. Sánchez-Arenillas, M.; Oujja, M.; Moutinho, F.; de la Figuera, J.; Cañamares, M.V.; Quesada, A.; Castillejo, M.; Marco, J.F. Bulk and Surface Characterisation of Micrometer-Thick Cobalt Ferrite Films Grown by IR PLD. *Appl. Surf. Sci.* **2019**, *470*, 917–922. [CrossRef]
12. Abe, M.; Tamaura, Y. Ferrite Plating in Aqueous Solution: New Technique for Preparing Magnetic Thin Film. *J. Appl. Phys.* **1984**, *55*, 2614–2616. [CrossRef]
13. Abe, M.; Tada, M.; Matsushita, N.; Shimada, Y. Phenomenological Theory of Permeability in Films Having No In-Plane Magnetic Anisotropy: Application to Spin-Sprayed Ferrite Films. *J. Appl. Phys.* **2006**, *99*, 08M907. [CrossRef]
14. Liu, H.; Yu, Z.; Fu, B.; Ran, M.; Wu, C.; Jiang, X.; Guo, R.; Lan, Z.; Sun, K. Anisotropic Growth and Magnetic Properties of Nickel–Zinc Ferrite Thin Film by Spin Spray Deposition. *Ceram. Int.* **2020**, *47*, 1318–1324. [CrossRef]
15. Ran, M.; Yu, Z.; Sun, K.; Wu, C.; Qing, H.; Liu, H.; Lan, Z.; Jiang, X. Effects of Aqueous Ethanol Solutions on the Structural and Magnetic Properties of NiZn Ferrite Thin Films Prepared by Spin-Spray Deposition. *Ceram. Int.* **2021**, *47*, 15520–15526. [CrossRef]
16. Ko, S.W.; Li, J.; Podraza, N.J.; Dickey, E.C.; Trolier-McKinstry, S. Spin Spray-Deposited Nickel Manganite Thermistor Films For Microbolometer Applications. *J. Am. Ceram. Soc.* **2011**, *94*, 516–523. [CrossRef]
17. Zhou, Z.; Obi, O.; Nan, T.X.; Beguhn, S.; Lou, J.; Yang, X.; Gao, Y.; Li, M.; Rand, S.; Lin, H.; et al. Low-Temperature Spin Spray Deposited Ferrite/Piezoelectric Thin Film Magnetoelectric Heterostructures with Strong Magnetoelectric Coupling. *J. Mater. Sci. Mater. Electron.* **2014**, *25*, 1188–1192. [CrossRef]
18. Obi, O.; Liu, M.; Lou, J.; Stoute, S.; Xing, X.; Sun, N.X.; Warzywoda, J.; Sacco, A.; Oates, D.E.; Dionne, G.F. Spin-Spray Deposited NiZn-Ferrite Films Exhibiting $\mu_r' > 50$ at GHz Range. *J. Appl. Phys.* **2011**, *109*, 07E527. [CrossRef]
19. Wang, X.; Zhou, Z.; Behugn, S.; Liu, M.; Lin, H.; Yang, X.; Gao, Y.; Nan, T.; Xing, X.; Hu, Z.; et al. Growth Behavior and RF/Microwave Properties of Low Temperature Spin-Sprayed NiZn Ferrite. *J. Mater. Sci. Mater. Electron.* **2015**, *26*, 1890–1894. [CrossRef]
20. Li, M.; Zhou, Z.; Liu, M.; Lou, J.; Oates, D.E.; Dionne, G.F.; Wang, M.L.; Sun, N.X. Novel NiZnAl-Ferrites and Strong Magnetoelectric Coupling in NiZnAl-Ferrite/PZT Multiferroic Heterostructures. *J. Phys. D Appl. Phys.* **2013**, *46*, 275001. [CrossRef]
21. Mirzaee, S.; Farjami shayesteh, S.; Mahdavifar, S.; Hekmatara, S.H. Synthesis, Characterization and Monte Carlo Simulation of CoFe2O4/Polyvinylpyrrolidone Nanocomposites: The Coercivity Investigation. *J. Magn. Magn. Mater.* **2015**, *393*, 1–7. [CrossRef]
22. Salcedo Rodríguez, K.L.; Bridoux, G.; Heluani, S.P.; Pasquevich, G.A.; Esquinazi, P.D.; Rodríguez Torres, C.E. Influence of Substrate Effects in Magnetic and Transport Properties of Magnesium Ferrite Thin Films. *J. Magn. Magn. Mater.* **2019**, *469*, 643–649. [CrossRef]
23. An, X.; Ingole, P.G.; Choi, W.-K.; Lee, H.-K.; Hong, S.U.; Jeon, J.-D. Development of Thin Film Nanocomposite Membranes Incorporated with Sulfated β-Cyclodextrin for Water Vapor/N_2 Mixture Gas Separation. *J. Ind. Eng. Chem.* **2018**, *59*, 259–265. [CrossRef]
24. Pradhan, D.K.; Kumari, S.; Pradhan, D.K.; Kumar, A.; Katiyar, R.S.; Cohen, R.E. Effect of Substrate Temperature on Structural and Magnetic Properties of C-Axis Oriented Spinel Ferrite $Ni_{0.65}Zn_{0.35}Fe_2O_4$ (NZFO) Thin Films. *J. Alloy. Compd.* **2018**, *766*, 1074–1079. [CrossRef]
25. Wu, Y.; Tang, Z.; Xu, Y.; Zhang, B.; He, X. A New Shorted Microstrip Method to Determine the Complex Permeability of Thin Films. *IEEE Trans. Magn.* **2010**, *46*, 886–888. [CrossRef]
26. Li, Y.F.; Li, E.; Zhang, Y.P.; Zhao, C.; Yang, T. Ultra-Wideband Variable Temperature Measurement System for Complex Permeability of Magnetic Thin Film $Fe_{66}Co_{17}B_{16}Si_1$. *IEEE Trans. Magn.* **2018**, *54*, 1–7. [CrossRef]
27. Nawle, A.C.; Humbe, A.V.; Babrekar, M.K.; Deshmukh, S.S.; Jadhav, K.M. Deposition, Characterization, Magnetic and Optical Properties of Zn Doped $CuFe_2O_4$ Thin Films. *J. Alloy Compd.* **2017**, *695*, 1573–1582. [CrossRef]
28. Brabers, V.A.M. Chapter 3 Progress in Spinel Ferrite Research. In *Handbook of Magnetic Materials*; Elsevier: Amsterdam, The Netherlands, 1995; Volume 8, pp. 189–324.
29. Taniguchi, A.; Taniguchi, T.; Wagata, H.; Katsumata, K.; Okada, K.; Matsushita, N. Liquid-Phase Atomic Layer Deposition of Crystalline Hematite without Post-Growth Annealing. *CrystEngComm* **2019**, *21*, 4184–4191. [CrossRef]
30. Khan, M.A.; Comyn, T.P.; Bell, A.J. Growth and Characterization of Tetragonal Bismuth Ferrite–Lead Titanate Thin Films. *Acta Mater.* **2008**, *56*, 2110–2118. [CrossRef]
31. Yang, S.; Chen, F.; Gao, X.; Shen, Q.; Zhang, L. Enhanced Power Factor of Textured Al-Doped-ZnO Ceramics by Field-Assisted Deforming. *J. Am. Ceram. Soc.* **2017**, *100*, 1300–1305. [CrossRef]
32. Wu, C.; Wang, W.; Li, Q.; Wei, M.; Luo, Q.; Fan, Y.; Jiang, X.; Lan, Z.; Jiao, Z.; Tian, Y.; et al. Barium hexaferrites with narrow ferrimagnetic resonance linewidth tailored by site-controlled Cu doping. *J. Am. Ceram. Soc.* **2022**, *105*, 7492–7501. Available online: https://ceramics.onlinelibrary.wiley.com/doi/abs/10.1111/jace.18702 (accessed on 3 March 2023). [CrossRef]
33. Kitayama, M.; Hirao, K.; Toriyama, M.; Kanzaki, S. Thermal Conductivity of SS-Si_3N_4: I, Effects of Various Microstructural Factors. *J. Am. Ceram. Soc.* **1999**, *82*, 3105–3112. [CrossRef]
34. Alben, R.; Becker, J.J.; Chi, M.C. Random Anisotropy in Amorphous Ferromagnets. *J. Appl. Phys.* **1978**, *49*, 1653–1658. [CrossRef]
35. Herzer, G. Anisotropies in Soft Magnetic Nanocrystalline Alloys. *J. Magn. Magn. Mater.* **2005**, *294*, 99–106. [CrossRef]

36. Mesbahinia, A.; Almasi-Kashi, M.; Ghasemi, A.; Ramezani, A. First Order Reversal Curve Analysis of Cobalt-Nickel Ferrite. *J. Magn. Magn. Mater.* **2019**, *473*, 161–168. [CrossRef]
37. Zheng, H.; Luo, J.; Wu, Q.; Zheng, P.; Zheng, L.; Han, M.; Zhang, Y. Hexagonal Barium Ferrite Films on a Pt(1 1 1)/Si(0 0 1) Substrate and Their Local Magnetic Properties. *J. Magn. Magn. Mater.* **2019**, *479*, 99–104. [CrossRef]
38. Zhang, Y.; Dai, B.; Li, J.; Zhu, H.; Zhu, X.; Li, X.; Ren, J.; Ren, Y. Break the Acher's Limit: Improve Both Resonance Frequency and Initial Permeability in Patterned FeNi Strip Film. *J. Alloy. Compd.* **2017**, *725*, 598–605. [CrossRef]
39. Jin, H.; Miyazaki, T. Soft Magnetism. In *The Physics of Ferromagnetism*; Miyazaki, T., Jin, H., Eds.; Springer Series in Materials Science; Springer: Berlin/Heidelberg, Germany, 2012; pp. 305–338; ISBN 978-3-642-25583-0.